IEEE Access
Multidisciplinary | Rapid Review | Open Access Journal

Received October 18, 2021, accepted December 13, 2021, date of publication December 14, 2021,
date of current version December 24, 2021.

Digital Object Identifier 10.1109/ACCESS.2021.3135763

MRAS-Based Induction Machine Magnetizing Inductance Estimator With Included Effect of Iron Losses and Load

ONDREJ LIPCAK, (Graduate Student Member, IEEE), AND JAN BAUER, (Member, IEEE)
Department of Electric Drives and Traction, Faculty of Electrical Engineering, Czech Technical University in Prague, 16627 Prague, Czech Republic

Corresponding author: Ondrej Lipcak (lipcaond@fel.cvut.cz)

This work was supported by the Student Grant Competition of the Czech Technical University in Prague under Grant SGS21/116/OHK3/2T/13.

ABSTRACT Although still widely used due to its robustness, reliability, and low cost, induction motor (IM) has a disadvantage of more complicated mathematical description than permanent magnet AC machines. In high-demanding applications, the decoupled control of the machine's flux and torque along with the proper function of selected efficiency-improving and flux-weakening algorithms can be achieved only if the IM parameters are known with sufficient accuracy. For parameter estimation, many algorithms have been proposed in the literature so far. Due to its simple and straightforward implementation, one of the popular estimation strategies is the model reference adaptive system (MRAS). However, MRAS-based algorithms for a specific parameter estimation tend to be sensitive to other machine parameters. For instance, most of the proposed MRAS algorithms do not consider the influence of the phenomena such as iron losses and load-dependent saturation. Since one of the most performance-decisive parameters of the popular rotor flux-oriented control (RFOC) are the magnetizing inductance and the rotor resistance, this paper aims to present a novel MRAS-based magnetizing inductance estimator (Lm-MRAS) with the included effect of iron losses. Furthermore, to enable the identification of the load-dependent saturation, another MRAS with included iron losses based on reactive power is proposed to work parallelly with Lm-MRAS, since under load conditions, the rotor resistance mismatch causes RFOC detuning. The adaptation law of the Lm-MRAS is obtained using the Lyapunov function approach and further examined using small-signal analysis. The proposed algorithms are verified on a 3.6 kW IM drive both in simulations and experiments.

INDEX TERMS Induction motor drives, iron losses, magnetizing flux saturation, model reference adaptive systems, parameter estimation, stability analysis.

I. INTRODUCTION

Real-time identification of induction machine (IM) parameters in the rotor flux-oriented control (RFOC) is still an ongoing topic amongst researchers in the field of electric drives and power electronics. For example, in the European Union, due to the emerging legislation and the growing societal demands, the requirements for the efficiency of electrical equipment are constantly increasing. Following this trend, the task of software engineers dealing with the control of electric drives is to design the most efficient software. Within the scope of the machine control, this essentially includes the compensation of various IM drive nonlinearities and deployment of control algorithms such as maximum torque per ampere (MTPA). However, many of the proposed efficiency-improving strategies are parameter-dependent [1], [2].

The traditional and widely used circuit is the so-called T-equivalent circuit which can be obtained using the space-vector theory of electrical machines. Furthermore, the equivalent circuit can be augmented to include the specific nonlinear phenomena such as magnetizing flux or rotor leakage flux saturation [4]–[7], iron losses [7], [8], or stray-load losses [9] that are difficult to capture at the stage of the mathematical derivation of machine's fundamental flux and voltage equations.

To ensure an effective operation of IM drives in high-demanding applications such as electric traction vehicles,

The associate editor coordinating the review of this manuscript and approving it for publication was Alfeu J. Sguarezi Filho.

precise decoupled control of the machine's flux and torque is needed. This demand goes hand in hand with the accurate knowledge of the IM parameters [10]. Also, an appropriate equivalent circuit that captures the most performance-decisive phenomena must be selected to obtain relevant results through the estimation algorithms.

For instance, although omitted in many papers, iron losses undoubtedly affect the IM RFOC [8], [10]. One way to respect the influence of iron losses is to add a fictitious resistance either in parallel or in series with the magnetizing branch [8]. Another phenomenon that is overlooked in many papers is load-dependent saturation. Due to the complicated distribution of the electromagnetic field inside the machine, the magnetizing flux can also saturate as a consequence of the load [11], especially if the rotor slots are skewed or closed [4]–[6]. Since the accurate knowledge of the magnetizing inductance has a decisive influence on the performance of the RFOC strategies, this nonlinear phenomenon should be respected in high-efficiency drives.

So far, many methods for the online identification of IM parameters have been proposed. These include recursive least-square algorithms (RLS) [12]–[14], model reference adaptive systems (MRAS) [15]–[21], signal injection (SI) techniques [22]–[24], state observers (SO) [25]–[27], and artificial intelligence (ANN) [28]–[30]. Typically, the greater the estimation accuracy and independence from other machine parameters, the greater the algorithm complexity, which demands sufficient computational power of the used hardware and the knowledge and experience of the implementation engineer. For example, methods based on MRAS that are quite popular within electric drives offer the comfort of ease of implementation but at the price of dependency on other machine parameters.

This paper aims to present a novel MRAS-type estimator for identifying both the no-load and load-dependent saturation of IM that can respect the effect of the machine's iron losses. The main disadvantage of the MRAS schemes, i.e., the dependence on other machine's parameters, can manifest itself during the load operation because, at load conditions, the rotor flux estimation depends on the rotor resistance [30]. This disadvantage is solved by utilizing a second, parallelly operating MRAS estimator based on the machine's reactive power that is also augmented to respect the iron losses.

The adaptation law of the magnetizing inductance MRAS estimator is designed using the Lyapunov function approach. Furthermore, a small-signal analysis is also presented to assess the stability of the estimator with respect to the controller gain selection. Simulations and experiments conducted on a 3.6 kW IM drive are presented to verify the proposed concept of magnetizing inductance identification.

II. INDUCTION MACHINE EQUIVALENT CIRCUIT

In this paper, the so-called T-equivalent circuit with included magnetizing flux saturation and equivalent iron loss resistance placed in parallel with the magnetizing inductance [31] depicted in Fig. 1 is utilized for the mathematical description of IM. In the figure, the symbols $\underline{\psi}_1$, $\underline{\psi}_2$ and $\underline{\psi}_\mathrm{m}$ represent the stator, rotor, and magnetizing flux linkage space vectors, respectively, $\underline{u}_1$ represents the stator voltage space vector, $\underline{i}_1$, $\underline{i}_2$, $\underline{i}_\mathrm{m}$ and $\underline{i}_\mathrm{Fe}$ represent the stator, rotor, magnetizing, and equivalent iron loss current space vectors, respectively, R_1, R_2, and R_Fe denote the stator, rotor, and equivalent iron loss resistance, respectively, ω_k is the electrical angular speed of the general reference frame, ω is the rotor electrical angular speed, L_m is the magnetizing inductance and the symbol j represents an imaginary unit ($\mathrm{j}^2 = -1$). A short-circuited rotor is considered; therefore, the rotor voltage equals zero. The stator inductance L_1 is defined as $L_1 = L_\mathrm{m} + L_{1\sigma}$, where $L_{1\sigma}$ is the stator leakage inductance and the rotor inductance L_2 is defined as $L_2 = L_\mathrm{m} + L_{2\sigma}$, where $L_{2\sigma}$ is the rotor leakage inductance.

The superscript k denotes that the space vectors are expressed in an arbitrary reference frame. The two specific reference frames used in this paper are the stator-fixed (real and imaginary axis denoted as α and β, respectively) and rotor flux vector-attached (real and imaginary axis denoted as d and q, respectively) reference frames.

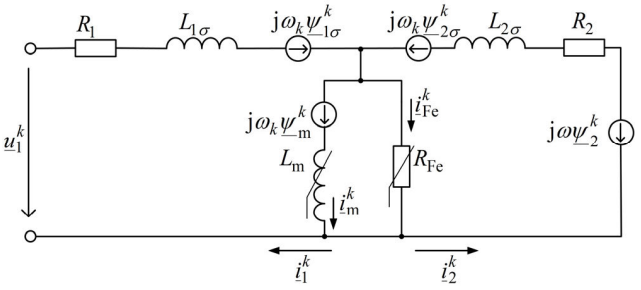

FIGURE 1. Induction machine T-equivalent circuit with included magnetizing inductance variation and iron losses.

A. STATE-SPACE MODEL WITH INCLUDED IRON LOSSES AND MAIN FLUX SATURATION

The full-order state space-model in the stationary $\alpha\beta$ reference frame with the current space vector, magnetizing space vector, and rotor space vector components as state variables is given by [10], [31]

$$\dot{\xi} = \mathbf{A}'\boldsymbol{\xi} + \mathbf{B}'\boldsymbol{v}, \tag{1}$$

where

$$\mathbf{A}' = \begin{pmatrix} a'_1 & 0 & a'_2 & 0 & a'_3 & 0 \\ 0 & a'_1 & 0 & a'_2 & 0 & a'_3 \\ R_\mathrm{Fe} & 0 & a'_4 & 0 & \tau^{-1}_{\mathrm{Fe}\sigma} & 0 \\ 0 & R_\mathrm{Fe} & 0 & a'_4 & 0 & \tau^{-1}_{\mathrm{Fe}\sigma} \\ 0 & 0 & \tau^{-1}_{\mathrm{r}\sigma} & 0 & -\tau^{-1}_{\mathrm{r}\sigma} & -\omega \\ 0 & 0 & 0 & \tau^{-1}_{\mathrm{r}\sigma} & \omega & -\tau^{-1}_{\mathrm{r}\sigma} \end{pmatrix}, \tag{2}$$

$$\mathbf{B}' = \begin{pmatrix} \frac{1}{L_{1\sigma}} & 0 & 0 & 0 & -\frac{1}{L_{1\sigma}} & 0 \\ 0 & \frac{1}{L_{1\sigma}} & 0 & 0 & 0 & -\frac{1}{L_{1\sigma}} \\ 0 & 0 & 0 & 0 & 1 & 0 \\ 0 & 0 & 0 & 0 & 0 & 1 \\ 0 & 0 & 1 & 0 & 0 & 0 \\ 0 & 0 & 0 & 1 & 0 & 0 \end{pmatrix}^{\mathrm{T}}, \tag{3}$$

$$\boldsymbol{\xi} = \begin{pmatrix} i_{1\alpha} & i_{1\beta} & \psi_{\mathrm{m}\alpha} & \psi_{\mathrm{m}\beta} & \psi_{2\alpha} & \psi_{2\beta} \end{pmatrix}^{\mathrm{T}}, \tag{4}$$

$$\boldsymbol{v} = \begin{pmatrix} u_{1\alpha} & u_{1\beta} & 0 & 0 & 0 & 0 \end{pmatrix}^{\mathrm{T}}, \tag{5}$$

and where $\tau_{\mathrm{r}\sigma} = L_{2\sigma}/R_2$, $\tau_{\mathrm{Fe}\sigma} = L_{2\sigma}/R_{\mathrm{Fe}}$, $a'_1 = -(R_1 + R_{\mathrm{Fe}})/L_{1\sigma}$, $a'_2 = L_2/(L_{1\sigma}L_{\mathrm{m}}\tau_{\mathrm{Fe}\sigma})$, $a'_3 = -1/(L_{1\sigma}\tau_{\mathrm{Fe}\sigma})$, $a_4 = -L_{1\sigma}a'_2$.

Considering Clarke's transformation constant equal to 2/3, the electromechanical torque can be expressed as

$$T_{\mathrm{e}} = \frac{3}{2}p_{\mathrm{p}}\frac{L_{\mathrm{m}}}{L_2}\left|\underline{\psi}_2^k \times \left(\underline{i}_1^k - \underline{i}_{\mathrm{Fe}}^k\right)\right|, \tag{6}$$

where p_{p} is the number of pole-pairs, and the operator $\times$ denotes cross product.

B. ROTOR FLUX ESTIMATION

The two standard IM reduced-order models used within the RFOC are the so-called current and voltage models. However, conventionally, these two models are derived out of the equivalent circuit with neglected iron losses. Therefore, in the following subsections, improved models with included iron losses will be presented.

1) CURRENT MODEL WITH INCLUDED IRON LOSSES

The model will be derived in an arbitrary reference frame. According to Fig. 1, the rotor voltage equation and the rotor flux linkage vector equation, respectively, can be expressed as

$$0 = R_2\underline{i}_2^k + \frac{\mathrm{d}\underline{\psi}_2^k}{\mathrm{d}t} + \mathrm{j}(\omega_k - \omega)\underline{\psi}_2^k, \tag{7}$$

$$\underline{\psi}_2^k = L_{2\sigma}\underline{i}_2^k + L_{\mathrm{m}}\underline{i}_{\mathrm{m}}^k = L_2\underline{i}_2^k + L_{\mathrm{m}}\left(\underline{i}_1^k - \underline{i}_{\mathrm{Fe}}^k\right). \tag{8}$$

Substituting for the rotor current vector in (7) from (8) yields after a few arrangements

$$\frac{\mathrm{d}\underline{\psi}_2^k}{\mathrm{d}t} = \frac{L_{\mathrm{m}}R_2}{L_2}\underline{i}_1'^k - \frac{R_2}{L_2}\underline{\psi}_2^k - \mathrm{j}(\omega_k - \omega)\underline{\psi}_2^k, \tag{9}$$

where $\underline{i}_1'^k = \underline{i}_1^k - \underline{i}_{\mathrm{Fe}}^k$. Considering the stator-fixed reference frame ($\omega_k = 0$), the model can be rewritten as

$$\frac{\mathrm{d}\underline{\psi}_2^{\alpha\beta}}{\mathrm{d}t} = \frac{L_{\mathrm{m}}R_2}{L_2}\underline{i}_1'^{\alpha\beta} - \frac{R_2}{L_2}\underline{\psi}_2^{\alpha\beta} + \mathrm{j}\omega\underline{\psi}_2^{\alpha\beta}. \tag{10}$$

Furthermore, choosing the rotor flux linkage vector-attached reference frame, one can obtain the steady-state expression for the rotor flux magnitude and slip frequency in the form

$$\psi_2 = L_{\mathrm{m}}i'_{1d}, \tag{11}$$

$$\omega_{\mathrm{sl}} = \frac{L_{\mathrm{m}}R_2}{L_2}\frac{i'_{1q}}{\psi_{2d}}, \tag{12}$$

where $\psi_2 = \psi_{2d} = \left|\underline{\psi}_2\right|$, $i'_{1d} = i_{1d} - i_{\mathrm{Fe}d}$, and $i'_{1q} = i_{1q} - i_{\mathrm{Fe}q}$.

2) VOLTAGE MODEL WITH INCLUDED IRON LOSSES

The model is almost exclusively used in the $\alpha\beta$ reference frame. According to Fig. 1, the stator flux linkage vector can be expressed as

$$\underline{\psi}_1^k = L_{1\sigma}\underline{i}_1^k + L_{\mathrm{m}}\underline{i}_{\mathrm{m}}^k = L_1\underline{i}_1^k + L_{\mathrm{m}}\left(\underline{i}_2^k - \underline{i}_{\mathrm{Fe}}^k\right). \tag{13}$$

Substituting for the rotor current vector in (8) from (13) and considering the stator-fixed reference frame yields

$$\underline{\psi}_2^{\alpha\beta} = \frac{L_2}{L_{\mathrm{m}}}\left(\underline{\psi}_1^{\alpha\beta} - L_{1\sigma}\underline{i}_1^{\alpha\beta}\right) + L_{2\sigma}\underline{i}_{\mathrm{Fe}}^{\alpha\beta}, \tag{14}$$

where $\sigma = 1 - L_{\mathrm{m}}^2/L_1L_2$ is the leakage factor. The stator flux linkage vector is obtained as

$$\underline{\psi}_1^{\alpha\beta} = \int_0^t \left(\underline{u}_1^{\alpha\beta} - R_1\underline{i}_1^{\alpha\beta}\right)\mathrm{d}\tau. \tag{15}$$

C. SENSITIVITY OF VOLTAGE MODEL TO MAGNETIZING INDUCTANCE VARIATION

The evaluation of the stator flux linkage vector using (15) is free of the magnetizing inductance. However, the magnetizing inductance appears in (14) when the stator flux linkage vector is recalculated to the rotor flux linkage vector. For convenience, new parameters containing the magnetizing inductance-dependent terms are introduced as

$$c_1 = \frac{L_2}{L_{\mathrm{m}}} = 1 + \frac{L_{2\sigma}}{L_{\mathrm{m}}}, \tag{16}$$

$$c_2 = L_1\sigma = L_{1\sigma} + \frac{L_{2\sigma}L_{\mathrm{m}}}{L_{\mathrm{m}} + L_{2\sigma}}. \tag{17}$$

The percentage change of these parameters with respect to the percentage deviation of the magnetization inductance ΔL_{m} from its nominal value can be written as

$$\Delta c_1 = \frac{L_{2\sigma}\Delta L_{\mathrm{m}}}{L_2\left(100 + \Delta L_{\mathrm{m}}\right)} \cdot 100, \tag{18}$$

$$\Delta c_2 = -\frac{L_{2\sigma}^2 L_{\mathrm{m}}\Delta L_{\mathrm{m}}}{\left(L_{2\sigma}L_{\mathrm{m}} + L_{1\sigma}L_2\right)\left(100L_2 + L_{\mathrm{m}}\Delta L_{\mathrm{m}}\right)} \cdot 100. \tag{19}$$

The dependencies $\Delta c_1 = f\left(\Delta L_{\mathrm{m}}\right)$ and $\Delta c_2 = f\left(\Delta L_{\mathrm{m}}\right)$ calculated using the nominal tested motor parameters (Table 1) are shown in Fig. 2. The variation of ΔL_{m} in the range of tens of percent causes the variation of the parameter only in the range of units of percent. Contrary to that, equation (11) states that if a steady-state is considered, then the variation of the magnetizing inductance directly proportional affects the output of the flux controller, i.e., d-axis current command.

III. PROPOSED MRAS-BASED MAGNETIZING INDUCTANCE ESTIMATOR WITH INCLUDED IRON LOSSES

The basic MRAS principle is that two mathematical models, the reference and adaptive, are evaluated parallelly. The reference model does not depend on the estimated quantity. On the contrary, the adaptive model utilizes directly or indirectly the estimated quantity. An adaptation mechanism

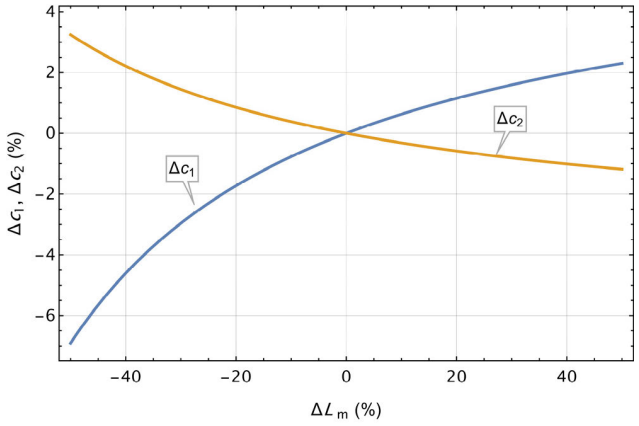

FIGURE 2. Percentage variation of the voltage model magnetizing inductance-dependent parameters due to percentage deviation of the magnetizing inductance from its nominal value.

(usually a simple PI controller) estimates the desired variable by forcing the difference between the reference and adaptive model to be zero. For the MRAS design, the Lyapunov theory or hyperstability theory can be utilized [19]. In this paper, the Lyapunov approach is adopted for the derivation of the adaptation mechanism

A. ADAPTATION MECHANISM DERIVATION USING LYAPUNOV THEORY

Let us consider a current model in the stationary reference frame, which utilizes the estimated magnetizing inductance $\hat{L}_\mathrm{m}$, i.e.,

$$\frac{\mathrm{d}\hat{\underline{\psi}}_2^{\alpha\beta}}{\mathrm{d}t} = \frac{\hat{L}_\mathrm{m}R_2}{\hat{L}_2}\underline{i}_1^{\alpha\beta} - \frac{R_2}{\hat{L}_2}\hat{\underline{\psi}}_2^{\alpha\beta} + \mathrm{j}\omega\hat{\underline{\psi}}_2^{\alpha\beta}, \tag{20}$$

where $\hat{L}_2 = \hat{L}_\mathrm{m} + L_{2\sigma}$. It is supposed that all the other parameters are known.

The error vector, i.e., the difference between the estimated and actual flux linkage space vector components, can be defined as

$$\boldsymbol{\varepsilon} = \begin{pmatrix} \varepsilon_\alpha \\ \varepsilon_\beta \end{pmatrix} = \begin{pmatrix} \psi_{2\alpha} - \hat{\psi}_{2\alpha} \\ \psi_{2\beta} - \hat{\psi}_{2\beta} \end{pmatrix}, \tag{21}$$

and its time derivative as

$$\dot{\boldsymbol{\varepsilon}} = \frac{\mathrm{d}}{\mathrm{d}t}\begin{pmatrix} \varepsilon_\alpha \\ \varepsilon_\beta \end{pmatrix} = \frac{\mathrm{d}}{\mathrm{d}t}\begin{pmatrix} \psi_{2\alpha} - \hat{\psi}_{2\alpha} \\ \psi_{2\beta} - \hat{\psi}_{2\beta} \end{pmatrix}. \tag{22}$$

By resolving (20) and (10) into their real and imaginary parts, respectively, and substituting the result into (22), one can obtain the error dynamics in the form

$$\dot{\boldsymbol{\varepsilon}} = \mathbf{H}\boldsymbol{\varepsilon} - \mathbf{W}, \tag{23}$$

where

$$\mathbf{H} = \begin{pmatrix} -\frac{R_2}{L_2} & -\omega \\ \omega & -\frac{R_2}{L_2} \end{pmatrix}, \tag{24}$$

$$\mathbf{W} = \begin{pmatrix} \frac{\Delta L_\mathrm{m}R_2}{\hat{L}_2L_2} & 0 & \frac{\Delta L_\mathrm{m}R_2L_{2\sigma}}{\hat{L}_2L_2} & 0 \\ 0 & \frac{\Delta L_\mathrm{m}R_2}{\hat{L}_2L_2} & 0 & \frac{\Delta L_\mathrm{m}L_{2\sigma}R_2}{\hat{L}_2L_2} \end{pmatrix} \times \begin{pmatrix} \hat{\psi}_{2\alpha} \\ \hat{\psi}_{2\beta} \\ i'_{1\alpha} \\ i'_{1\beta} \end{pmatrix}, \tag{25}$$

and where $\Delta L_\mathrm{m} = L_\mathrm{m} - \hat{L}_\mathrm{m}$.

Now, let us consider the Lyapunov function candidate [16], [32]

$$V = \boldsymbol{\varepsilon}^\mathrm{T}\boldsymbol{\varepsilon} + \frac{\Delta L_\mathrm{m}^2}{\delta}, \tag{26}$$

and its time derivative

$$\dot{V} = \boldsymbol{\varepsilon}^\mathrm{T}\left(\mathbf{H}^\mathrm{T}+\mathbf{H}\right)\boldsymbol{\varepsilon} - \boldsymbol{\varepsilon}^\mathrm{T}\mathbf{W} - \mathbf{W}^\mathrm{T}\boldsymbol{\varepsilon} - \frac{2\Delta L_\mathrm{m}}{\delta}\frac{\mathrm{d}\hat{L}_\mathrm{m}}{\mathrm{d}t}, \tag{27}$$

where δ is a positive parameter.

By expanding the term containing the matrix $\mathbf{H}$, it can be verified that it is non-positive, i.e.,

$$\boldsymbol{\varepsilon}^\mathrm{T}\left(\mathbf{H}^\mathrm{T}+\mathbf{H}\right)\boldsymbol{\varepsilon} = -\frac{2R_2}{L_2}\left(\varepsilon_\alpha^2 + \varepsilon_\beta^2\right) \leq 0. \tag{28}$$

The sufficient condition for the stability is that the remaining term at least satisfy the condition [16], [32]

$$-\boldsymbol{\varepsilon}^\mathrm{T}\mathbf{W} - \mathbf{W}^\mathrm{T}\boldsymbol{\varepsilon} - \frac{2\Delta L_\mathrm{m}}{\delta}\frac{\mathrm{d}\hat{L}_\mathrm{m}}{\mathrm{d}t} = 0. \tag{29}$$

Substituting (24) and (25) into (29), the inductance estimate time derivative can be expressed as

$$\frac{\mathrm{d}\hat{L}_\mathrm{m}}{\mathrm{d}t} = \frac{\delta R_2}{\hat{L}_2L_2}\left[\varepsilon_\alpha\left(\hat{\psi}_{2\alpha}+L_{2\sigma}i'_{1\alpha}\right) + \varepsilon_\beta\left(\hat{\psi}_{2\beta}+L_{2\sigma}i'_{1\beta}\right)\right]. \tag{30}$$

Out of (30), the adaptation law in the form of an I controller directly follows. In practice, a PI controller is used for better dynamic performance [19], [32]. The resulting magnetizing inductance MRAS-type estimator can be written as

$$\hat{L}_\mathrm{m} = K_{\mathrm{P}\psi}\varepsilon_\psi^{\alpha\beta} + K_{\mathrm{I}\psi}\int_0^t \varepsilon_\psi^{\alpha\beta}\mathrm{d}\tau + L_{\mathrm{m(init)}}, \tag{31}$$

where $L_{\mathrm{m(init)}}$ is the initial magnetizing inductance value and

$$\varepsilon_\psi^{\alpha\beta} = \varepsilon_\alpha\left(\hat{\psi}_{2\alpha}+L_{2\sigma}i'_{1\alpha}\right) + \varepsilon_\beta\left(\hat{\psi}_{2\beta}+L_{2\sigma}i'_{1\beta}\right). \tag{32}$$

Due to the low sensitivity to magnetizing inductance variation, the voltage model (equations (14) and (15)) is selected as the reference model, and the current model (equation (20)) is selected as the adaptive model. The block diagram of the proposed estimator is depicted in Fig. 3.

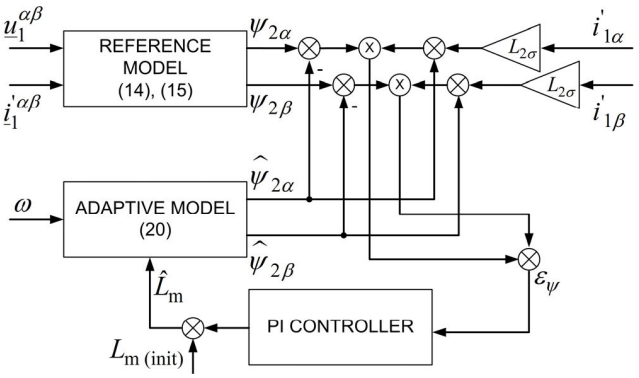

FIGURE 3. MRAS for magnetizing inductance estimation with the included effect of iron losses.

B. SMALL SIGNAL ANALYSIS

The stability with respect to the adaptive controller gain constants can be investigated using the linearization approach, which permits the system analysis via transfer functions [33]. For this purpose, a state-space model with the rotor flux linkage space vector and stator current space vector components is utilized. However, to obtain mathematically reasonable expressions, several simplifications and modifications must be adopted, namely:

- For the small-signal analysis, the equations must be transformed to a rotor flux-attached dq reference frame [33].
- Initially, the perfect flux orientation (zero q axis component) is considered for both the reference and adaptive model.
- The rotor flux linkage vector components from the adaptive model are considered ideal and constant.
- The analysis neglects iron losses since the state-space models with iron losses are mathematically more complicated.
- The influence of the dynamic inductances in the state-space model is neglected.

The full-order IM state-space model is considered in the form [18]

$$\dot{\mathbf{x}} = \mathbf{A}\mathbf{x} + \mathbf{B}\mathbf{u}, \tag{33}$$

$$\mathbf{y} = \mathbf{C}\mathbf{x}, \tag{34}$$

where

$$\mathbf{A} = \begin{pmatrix} a_1 & \omega_\mathrm{s} & a_2 & a_3\omega \\ -\omega_\mathrm{sl} & a_1 & -a_3\omega & a_2 \\ a_4 & 0 & a_5 & \omega_\mathrm{sl} \\ 0 & a_4 & -\omega_\mathrm{sl} & a_5 \end{pmatrix}, \tag{35}$$

$$\mathbf{B} = \begin{pmatrix} 0 & \frac{1}{L_1\sigma} & 0 & 0 \\ \frac{1}{L_1\sigma} & 0 & 0 & 0 \end{pmatrix}^\mathrm{T}, \tag{36}$$

$$\mathbf{C} = \begin{pmatrix} 1 & 0 & 0 & 0 \\ 0 & 1 & 0 & 0 \end{pmatrix}, \tag{37}$$

$$\mathbf{x} = \begin{pmatrix} i_{1d} & i_{1q} & \psi_{2d} & \psi_{2q} \end{pmatrix}^\mathrm{T}, \tag{38}$$

$$\mathbf{u} = \begin{pmatrix} u_{1d} & u_{1q} \end{pmatrix}^\mathrm{T}, \tag{39}$$

$$\mathbf{y} = \begin{pmatrix} i_{1d} & i_{1q} \end{pmatrix}^\mathrm{T}, \tag{40}$$

and where $a_1 = -\left(R_1L_2^2 + L_\mathrm{m}^2R_2\right)/(\sigma L_1L_2^2)$, $a_2 = (L_\mathrm{m}R_2)/(\sigma L_1L_2^2)$, $a_3 = L_\mathrm{m}/(\sigma L_1L_2)$, $a_4 = (L_\mathrm{m}R_2)/L_2$, $a_5 = -R_2/L_2$, and ω_s is the synchronous speed.

Linearizing (33) and (34) around the operating point $\mathbf{x}_0 = \begin{pmatrix} i_{1d0} & i_{1q0} & \psi_{2d0} & \psi_{2q0} \end{pmatrix}^\mathrm{T}$ and L_m0 yields

$$\Delta\dot{\mathbf{x}} = \Delta\mathbf{A}_\mathrm{L}\mathbf{x}_0 + \mathbf{A}\Delta\mathbf{x} + \Delta\mathbf{B}_\mathrm{L}\mathbf{u}, \tag{41}$$

$$\Delta\mathbf{y} = \mathbf{C}\Delta\mathbf{x}, \tag{42}$$

where $\Delta\mathbf{x} = x - \mathbf{x}_0$ and

$$\Delta\mathbf{A}_\mathrm{L} = \left(\frac{\partial}{\partial L_\mathrm{m}}\mathbf{A}\right)\Delta L_\mathrm{m}, \tag{43}$$

$$\Delta\mathbf{B}_\mathrm{L} = \left(\frac{\partial}{\partial L_\mathrm{m}}\mathbf{B}\right)\Delta L_\mathrm{m}, \tag{44}$$

where $\Delta L_\mathrm{m} = L_\mathrm{m} - L_\mathrm{m0}$. After performing Laplace transform, (42) can be rewritten with the help of (41) as

$$\Delta\mathbf{y} = \begin{pmatrix} \Delta i_{1d} \\ \Delta i_{1q} \end{pmatrix} = \mathbf{C}\left(s\mathbf{I} - \mathbf{A}\right)^{-1}\left(\Delta\mathbf{A}_\mathrm{L}\mathbf{x}_0 + \Delta\mathbf{B}_\mathrm{L}\mathbf{u}\right), \tag{45}$$

where s is the Laplace operator, $\Delta i_{1d} = i_{1d} - i_{1d0}$, $\Delta i_{1q} = i_{1q} - i_{1q0}$, and $\mathbf{I}$ is the identity matrix. Equation (45) can be utilized to obtain the expressions for Δi_{1d} and Δi_{1q} (used further in the section).

The error equation (32) with neglected iron losses transformed into dq reference frame takes the form

$$\varepsilon_\psi^{dq} = \varepsilon_d\left(\hat{\psi}_{2d} + L_{2\sigma}i_{1d}\right) + \varepsilon_q\left(\hat{\psi}_{2q} + L_{2\sigma}i_{1q}\right). \tag{46}$$

Now, (46) must be linearized around an operating point $\hat{\psi}_{2d0}$, $\hat{\psi}_{2q0}$, ψ_{2d0}, ψ_{2q0}, i_{1d0}, i_{1q0}. Under the above assumptions it follows that $\hat{\psi}_{2d0} = \psi_{2d0} = \psi_{2d}$, $\hat{\psi}_{2q0} = \psi_{2q0} = \psi_{2q} = 0$. The linearized error equation can be then expressed as

$$\Delta\varepsilon_\psi^{dq} = -\left(L_{2\sigma}i_{1d0} + \hat{\psi}_{2d0}\right)\Delta\hat{\psi}_{2d}, \tag{47}$$

where $\Delta\hat{\psi}_{2d} = \hat{\psi}_{2d} - \hat{\psi}_{2d0}$.

Transforming the current model (9) into the dq reference frame, neglecting the iron losses, and using the slip speed equation (12), the model now becomes

$$\frac{\mathrm{d}\underline{\psi}_2^{dq}}{\mathrm{d}t} = \frac{L_\mathrm{m}R_2}{L_2}\underline{i}_1^{dq} - \frac{R_2}{L_2}\underline{\psi}_2^{dq} - \mathrm{j}\frac{L_\mathrm{m}R_2}{L_2}\frac{i_{1q}}{\psi_{2d}}\underline{\psi}_2^{dq}. \tag{48}$$

Linearizing (48) around the operating point $\hat{\psi}_{2d0}$, $\hat{\psi}_{2q0}$, i_{1d0}, i_{1q0}, and L_m0, separating the result into the real and imaginary part, respectively, and performing the Laplace transform, (48) can be rewritten as

$$\Delta\hat{\psi}_{2d}s = \frac{R_2L_\mathrm{m0}}{L_{20}}\Delta i_{1d} - \frac{R_2}{L_{20}}\Delta\hat{\psi}_{2d} + \frac{L_\mathrm{m0}R_2i_{1q0}}{L_{20}\psi_{2d0}}\Delta\hat{\psi}_{2q} + \frac{R_2\left(L_{2\sigma}i_{1d0} + \hat{\psi}_{2d0}\right)}{L_{20}^2}\Delta L_\mathrm{m}, \tag{49}$$

$$\Delta\hat{\psi}_{2q}s = -\frac{R_2}{L_{20}}\Delta\hat{\psi}_{2q}, \tag{50}$$

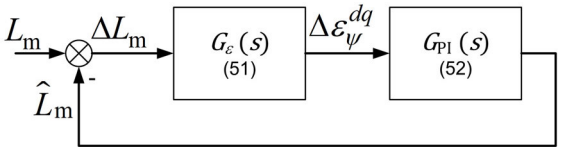

FIGURE 4. A block diagram of the linearized Lm-MRAS.

where $L_{20} = L_{m0} + L_{2\sigma}$. The error transfer function can be written as

$$G_\varepsilon(s) = -\frac{\Delta\varepsilon_\psi^{dq}}{\Delta L_m} = \left(L_{2\sigma} i_{1d0} + \hat{\psi}_{2d0}\right) \frac{\Delta\hat{\psi}_{2d}}{\Delta L_m}. \quad (51)$$

Resolving $\Delta\hat{\psi}_{2d}$ out of (49) and (50), substituting the result into (51) and also using (45) to substitute for the newly formed expression $\Delta i_{1d}/\Delta L_m$, the final error transfer function can be obtained. Due to its complexity, this equation is not explicitly stated in the paper.

The adaptive PI controller transfer function is considered in the form

$$G_{PI}(s) = K_{P\psi} + \frac{K_{I\psi}}{s}. \quad (52)$$

Therefore, the closed-loop transfer function of the whole estimator can be written as

$$G_C(s) = \frac{G_{PI}(s)\, G_\varepsilon(s)}{1 + G_{PI}(s)\, G_\varepsilon(s)}. \quad (53)$$

The block diagram of the linearized estimator is depicted in Fig. 4. Fig. 5 and Fig. 6 show the root locus of (53) for nominal parameters, nominal excitation, and a nominal load of the IM utilized in the simulations and experiments (nameplate values and model parameters given in Table 1). Fig. 5 for the case when $K_{P\psi} = 1$ and $K_{I\psi}$ changes within $\langle 0, 300\rangle$, and Fig. 6 for the case when $K_P = 0$ and K_I changes again within $\langle 0, 300\rangle$. In all these cases, the estimator remains stable.

Furthermore, (53) can also be used for the design of the adaptive controller gain constants. However, given the number of adopted simplifications and the fact that linearization is valid only around a specific operating point, the obtained results should be considered only as starting values that must be carefully adjusted.

C. SENSITIVITY TO ROTOR RESISTANCE VARIATION

Unfortunately, the proposed Lm-MRAS is sensitive to the rotor resistance variation. The sensitivity function can be obtained using a similar procedure to the one described in the previous section.

According to Fig. 4, the expression for ΔL_m can be obtained as

$$\Delta L_m = -\left(K_{P\psi} + \frac{K_{I\psi}}{s}\right) \Delta\varepsilon_\psi^{dq}. \quad (54)$$

The sensitivity function can be then expressed as

$$\frac{\Delta L_m}{\Delta R_2} = \left(K_{P\psi} + \frac{K_{I\psi}}{s}\right) \left(L_{2\sigma} i_{1d0} + \hat{\psi}_{2d0}\right) \frac{\Delta\hat{\psi}_{2d}}{\Delta R_2}. \quad (55)$$

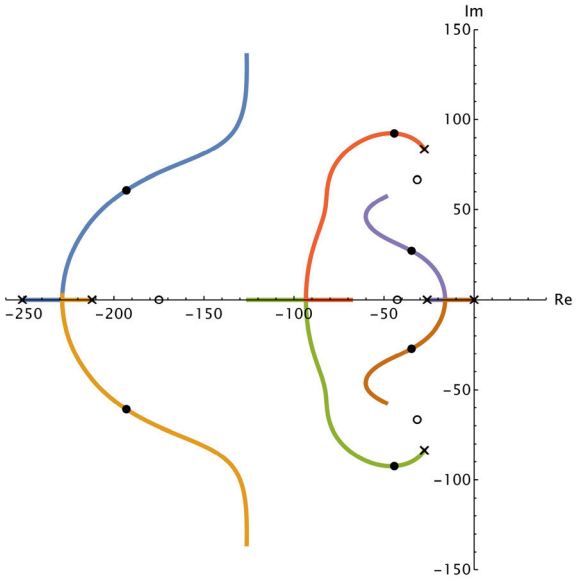

FIGURE 5. Root locus of the linearized L_m MRAS-type estimator, $K_{P\psi} = 1$ and $K_{I\psi}$ changes from 0 to 300; nominal excitation and speed, half of the nominal load torque. Crosses, dots, and circles represent the roots for the starting value, value in the middle of the interval, and value in infinity, respectively.

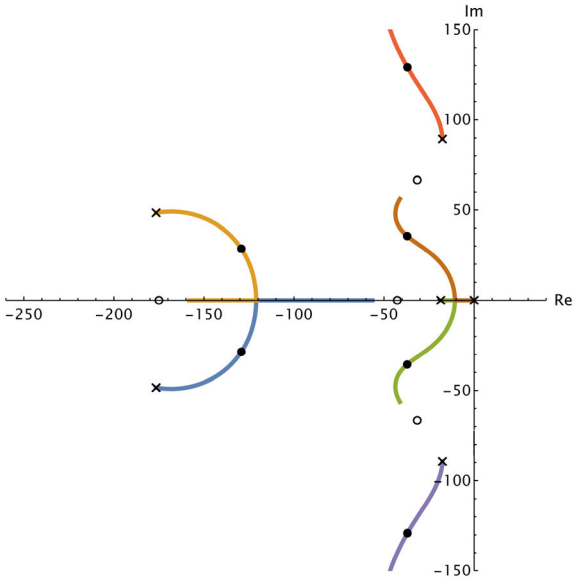

FIGURE 6. Root locus of the linearized L_m MRAS-type estimator, $K_{P\psi} = 0$ and $K_{I\psi}$ changes from 0 to 300; nominal excitation and speed, half of the nominal load torque. Crosses, dots, and circles represent the roots for the starting value, value in the middle of the interval, and value in infinity, respectively.

Using (48), the expressions for $\Delta\hat{\psi}_{2d}$ can be obtained similarly as in the previous section. However, this time the linearization is performed around the operating point $\hat{\psi}_{2d0}$, $\hat{\psi}_{2q0}$, i_{1d0}, i_{1q0}, L_{m0}, and R_{20}. To substitute for the newly formed expression $\Delta i_{1d}/\Delta R_2$, state-space model (33) and (34) is linearized around the operating point $\mathbf{x}_0 = \left(i_{1d0}\ i_{1q0}\ \psi_{2d0}\ \psi_{2q0}\right)^T$ and R_{20}. The resulting expression for

the output vector is

$$\Delta \mathbf{y} = \begin{pmatrix} \Delta i_{1d} \\ \Delta i_{1q} \end{pmatrix} = \mathbf{C}\left(s\mathbf{I} - \mathbf{A}\right)^{-1} \mathbf{\Delta A}_{\mathrm{R}} \mathbf{x}_0, \tag{56}$$

where

$$\mathbf{\Delta A}_{\mathrm{R}} = \left(\frac{\partial}{\partial R_2}\mathbf{A}\right) \Delta R_2. \tag{57}$$

After these operations, the resulting sensitivity function can be obtained. Fig. 7 shows the step response of the sensitivity function to the 10 % decrease in the rotor resistance. The PI controller parameters are selected as $K_{\mathrm{P}\psi} = 0.01$ and $K_{\mathrm{I}\psi} = 1$. Nominal excitation, speed, and load torque are considered.

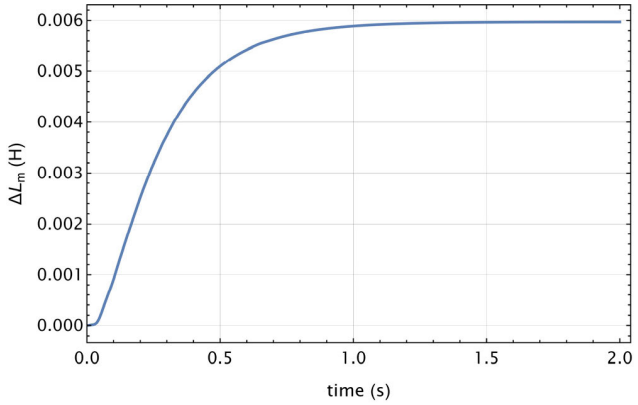

FIGURE 7. Step response of the rotor resistance sensitivity function to 10% decrease in the rotor resistance, $K_{P\psi} = 0.01$ and $K_{I\psi} = 1$. Nominal excitation, speed, and load torque.

IV. MEASUREMENT, MODELLING, AND COMPENSATION OF IRON LOSSES

Considering arbitrary reference frame, the equivalent iron loss current can be expressed according to Fig. 1 as

$$\underline{i}^{k}_{\mathrm{Fe}} = \frac{\underline{u}^{k}_{\mathrm{m}}}{R_{\mathrm{Fe}}}, \tag{58}$$

where $\underline{u}^{k}_{\mathrm{m}}$ is the voltage across the magnetizing (parallel) branch.

Considering Clarke's transformation constant equal to 2/3, the power dissipated in the iron core is given by

$$P_{\mathrm{Fe}} = \frac{3}{2}\Re\left\{\underline{u}^{k}_{\mathrm{m}}\bar{\underline{i}}^{k}_{\mathrm{Fe}}\right\}, \tag{59}$$

where $\bar{\underline{i}}^{k}_{\mathrm{Fe}}$ denotes the complex conjugate of the equivalent iron loss current. Substituting (58) into (59), the iron loss resistance can be expressed as

$$R_{\mathrm{Fe}} = \frac{3}{2}\frac{u^2_{\mathrm{m}}}{P_{\mathrm{Fe}}}. \tag{60}$$

Substituting (60) into (58) and considering the stationary reference, the iron loss current is obtained as

$$\underline{i}^{\alpha\beta}_{\mathrm{Fe}} = \frac{2}{3}P_{\mathrm{Fe}}\frac{\underline{u}^{\alpha\beta}_{\mathrm{m}}}{u^2_{\mathrm{m}}}. \tag{61}$$

The voltage across the magnetizing branch can be expressed in case of a steady-state operation and sinusoidal supply as

$$\underline{u}^{\alpha\beta}_{\mathrm{m}} = \underline{u}^{\alpha\beta}_{1} - R_1\underline{i}^{\alpha\beta}_{1} - \mathrm{j}\omega_{\mathrm{s}}L_{1\sigma}\underline{i}^{\alpha\beta}_{1}. \tag{62}$$

The measurement of iron losses and their implementation into the control algorithm will be discussed in the next section.

A. MEASUREMENT AND MODEL FITTING

The iron losses can be obtained by a series of no-load tests at various fundamental supply frequencies. The separation procedure based on the IEC standard can then be used for the loss calculation [34]. For the measurement, the inverter is programmed to generate a fundamental voltage at a given frequency and magnitude that corresponds to the reference stator flux linkage vector magnitude (obtained from the voltage model).

Out of the measured input power P_{in}, the iron losses are calculated as

$$P_{\mathrm{Fe}} = P_{\mathrm{c}} - P_{\mathrm{fw}}, \tag{63}$$

where P_{c} are the constant losses defined as

$$P_{\mathrm{c}} = P_0 - P_{\mathrm{s},0}, \tag{64}$$

where P_0 is the fundamental component of the input no-load power, $P_{\mathrm{s},0}$ are the stator copper losses calculated from the known value of the stator resistance and measured RMS current, and P_{fw} are the friction and windage losses, i.e., the mechanical losses.

The mechanical losses are calculated from four or more constant loss points between 30 % and 60 % of the rated motor stator flux by developing a curve against no-load voltage squared and then performing linear extrapolation to zero voltage [34]. The intersection of the extrapolation line with the vertical axis then corresponds to the mechanical losses.

For the iron loss modeling, the following analytical function is adopted [7]

$$P_{\mathrm{Fe}} = \frac{f_{\mathrm{s}}^2\psi_1^2 + \kappa f_{\mathrm{s}}\psi_1^n}{R_{\mathrm{Fe0}}}, \tag{65}$$

where f_{s} is the fundamental supply frequency and κ, n and R_{Fe0} are the model parameters. The measured iron losses are then fitted to the model using Wolfram Mathematica's command *NMinimize* with the *RandomSearch* option. The minimization is performed on a sum of squares of the error. The fitted dependence of the iron losses on the stator flux linkage vector magnitude and fundamental supply frequency is depicted in Fig. 8. The found model parameters are presented in the figure caption.

The iron losses are also a function of the slip [9]. If more precise results are required, an appropriate model considering the slip dependence can be used.

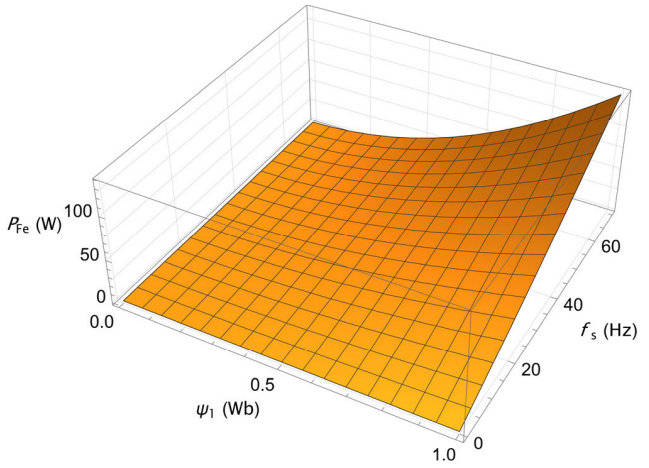

FIGURE 8. Iron losses as a function of fundamental supply frequency and stator flux linkage vector amplitude. The fitted model parameters are $R_{Fe0} = 277$, $\kappa = 460$, $n = 1.77$.

B. REAL-TIME COMPENSATION

In the control algorithm, the iron losses are calculated based on the estimated synchronous frequency and stator flux linkage vector amplitude. The synchronous frequency is obtained using the measured rotor speed and estimated slip speed (equation (12)), and the stator flux amplitude is calculated using the voltage model (equation (15)).

The resulting block diagram of the proposed FOC is depicted in Fig. 9.

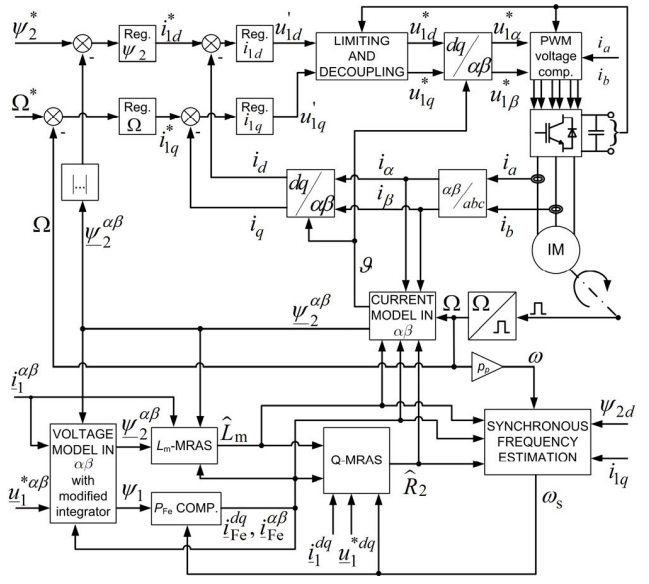

FIGURE 9. Block diagram of the proposed field-oriented control with the iron losses, magnetizing inductance, and rotor resistance compensation.

V. SELECTED IMPLEMENTATION ISSUES

A few problems arise during the practical implementation of the FOC along with the presented estimation algorithms. The two most important ones – DC offset accumulation problem during pure integration and inverter voltage distortion will be discussed in the following sections.

A. VOLTAGE MODEL – DC OFFSET ACCUMULATION IN CASE OF PURE INTEGRATION

First, it is not possible to use a pure integrator for the voltage model (eq. (15)) evaluation because of the unknown initial conditions and DC offset accumulation problem [35]. However, an advanced modified integrator based on the current model depicted in Fig. 10 can be used since the current model is also implemented in the control algorithm. The main drawback of this type of integrator is that it utilizes another PI controller, for which no satisfactory gain design method has been proposed yet. Therefore, before drive commissioning, the controller should be tuned adequately in the simulation model.

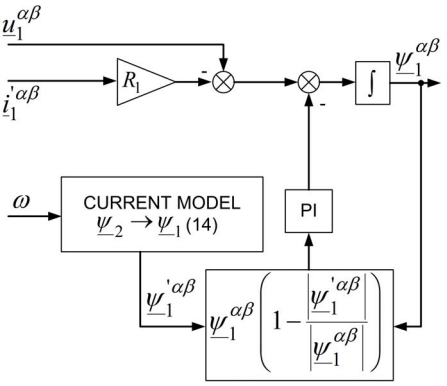

FIGURE 10. Current model-based modified integrator with the DC offset elimination.

B. INVERTER OUTPUT VOLTAGE DISTORTION

Another major issue that impairs the performance of all the advanced AC drive control strategies, if not accounted for, is the distortion of the inverter output voltage [36]. The primary sources of the voltage distortion are the inserted dead-time and the delayed load current-dependent transistor switching. It is assumed that the most common space-vector modulation (SVM) with a constant switching period T_{PWM} is used. The resulting effective dead-time that needs to be compensated is defined as [37]

$$T_{eff}(i_x) = T_{dt} + T_{on}(i_x) - T_{off}(i_x) \quad x = a, b, c, \quad (66)$$

where T_{dt} is the dead-time inserted by the microcontroller or driver, $T_{on}(i_x)$ is the current-dependent turn-on delay, $T_{off}(i_x)$ is the current-dependent turn-off delay and symbols a, b, c denote the respective inverter leg.

The compensation characteristics in the form of the dependence of the so-called effective dead-time on the load current can be easily determined by direct measurement [37]. In the control algorithm, a look-up table can be used for the effective

dead-time compensation, or it is possible to fit the measured data using the function

$$T_{\text{eff}}(i_x) = \frac{m}{k_1 |i_x| + k_2} + n, \tag{67}$$

where k_1, k_2, m, n are parameters to be determined.

The most convenient way is to compensate the output duty-cycle from the modulator [37]. Within SVM, the duty-cycle d_x for each VSI leg is defined in such a way that the average value of the corresponding inverter line-to-neutral voltage u_{x0} per modulation period with respect to given DC-link voltage U_{DC} equals to $-U_{\text{DC}}/2$ if $d_x = 0$ and $+U_{\text{DC}}/2$ if $d_x = 1$. The relation between the reference d_x^* and the compensated duty cycle d_x' then takes the following form [37]

$$d_x' = d_x^* + \frac{T_{\text{eff}(x)}}{T_{\text{PWM}}} \text{sgn}(i_x) \quad x = a, b, c. \tag{68}$$

VI. Q-MRAS FOR ROTOR RESISTANCE ESTIMATION, LOAD-DEPENDENT SATURATION

As mentioned in the Introduction, the IM magnetizing inductance may also depend on the load. Theoretically, the proposed Lm-MRAS with included iron losses should be capable of estimating this type of saturation. However, as shown in section III. C., another parameter that affects the accuracy of the current model and, consequently, the performance of the RFOC during the load conditions is the rotor resistance. Therefore, rotor resistance adaptation could improve the identification process. For this purpose, the traditional and widely used reactive power MRAS (Q-MRAS) can be utilized. In this paper, this type of estimator will be augmented to include the iron loss effect to improve the estimation accuracy further.

The reference model is given by [19]

$$Q = \Im \left\{ \underline{u}_1^{dq} \underline{\bar{i}}_1^{dq} \right\} = u_{1q} i_{1d} - u_{1d} i_{1q}, \tag{69}$$

where $\underline{\bar{i}}_1^{dq}$ denotes the conjugated current space vector. Using (14) transformed into dq reference frame, the stator flux linkage vector can be obtained as

$$\underline{\psi}_1^{dq} = \frac{L_{\text{m}}}{L_2} \underline{\psi}_2^{dq} + L_1 \sigma \underline{i}_1^{dq} - \frac{L_{2\sigma} L_{\text{m}}}{L_2} \underline{i}_{\text{Fe}}^{dq}. \tag{70}$$

The stator voltage equation in the dq reference frame can be written as

$$\underline{u}_1^{dq} = R_1 \underline{i}_1^{dq} + \frac{\text{d}\underline{\psi}_1^{dq}}{\text{d}t} + \text{j}\omega_{\text{s}} \underline{\psi}_1^{dq}. \tag{71}$$

By substituting (70) into (71) and considering the steady-state operation, we obtain

$$\underline{u}_1^{dq} = R_1 \underline{i}_1^{dq} + \text{j}\omega_s \left(\frac{L_{\text{m}}}{L_2} \underline{\psi}_2^{dq} + L_1 \sigma \underline{i}_1^{dq} - \frac{L_{2\sigma} L_{\text{m}}}{L_2} \underline{i}_{\text{Fe}}^{dq} \right). \tag{72}$$

Separating (72) into the real and imaginary parts, respectively, while considering that $\psi_{2d} = L_{\text{m}}(i_{1d} - i_{\text{Fe}d})$ and $\psi_{2q} = 0$, the adaptive model is finally obtained as

$$\hat{Q} = \omega_{\text{s}} \Big[L_1 \sigma \left(i_{1d}^2 + i_{1q}^2 \right) + \frac{L_{\text{m}}}{L_2} \left(L_{\text{m}} i_{1d}^2 - L_2 i_{\text{Fe}d} i_{1d} - L_{2\sigma} i_{\text{Fe}q} i_{1q} \right) \Big]. \tag{73}$$

The synchronous speed is obtained as the sum of the measured speed and estimated slip speed.

The error for the rotor resistance adaptation mechanism is calculated as

$$\varepsilon_Q = Q - \hat{Q}. \tag{74}$$

The estimated rotor resistance is then the output of the PI controller, i.e.,

$$\hat{R}_2 = K_{\text{p}Q} \varepsilon_Q + K_{\text{i}Q} \int_0^t \varepsilon_Q \text{d}\tau + R_{2(\text{init})}, \tag{75}$$

where $R_{2(\text{init})}$ is the initial rotor resistance. The block diagram of the Q-MRAS estimator with included iron loss effect is presented in Fig. 11.

The stability analysis of the parallel operation of the Lm-MRAS and Q-MRAS represents a complex task. Generally, no satisfactory approach to investigating multiple simultaneous MRAS-type estimators' stability within FOC has been proposed yet. The analysis is usually omitted or greatly simplified [17].

VII. SIMULATION RESULTS

The simulation model was built in MATLAB/Simulink version 2021a. The simulated machine nameplate values and nominal model parameters are given in Table 1. The block diagram of the control algorithm agrees with Fig. 9. The selected model solver is *ode4* with a fixed-step size equal to 5 μs. The machine is modeled using the full-order state-space model with the iron loss effect presented in section II. A. The iron losses are calculated using (65) fitted to the measured data.

To eliminate the effect of numerical errors and the effect of the pulse voltage (i.e., the effect of the inverter) on the estimator accuracy, the model of FOC is implemented using the same solver and fixed-step size as in the case of the IM model. The stator flux linkage vector magnitude and the slip speed for the iron loss compensation (utilizing (65) again) are calculated using the voltage model (15) and the slip speed equation (12), respectively.

To assess the functionality of the proposed estimator, the following sequence is simulated:

- The magnetizing inductance in the FOC model is set to 110 % of the nominal value. All other parameters are exact.
- The reference flux is set to the nominal value.
- The machine is started at 0.1 s to half of the nominal speed. The reference speed is increased to the nominal value at 4 s.

- Magnetizing inductance compensation is turned on at 1 s.
- Initially, the machine is unloaded. The load is increased to half of the nominal torque and nominal torque at 2 s and 3 s, respectively. Furthermore, the load is decreased to half of the nominal torque and zero torque at 5 s and 6 s, respectively.

The time sequence of the step changes of the reference speed and torque is depicted in Fig. 12. The Lm-MRAS PI controller proportional and integral gains are set to 0.01 and 1, respectively. The resulting magnetizing inductance estimates are depicted in Fig. 13 and Fig. 14. In Fig. 13, the iron losses are compensated, and in Fig. 14, the compensation is inactive.

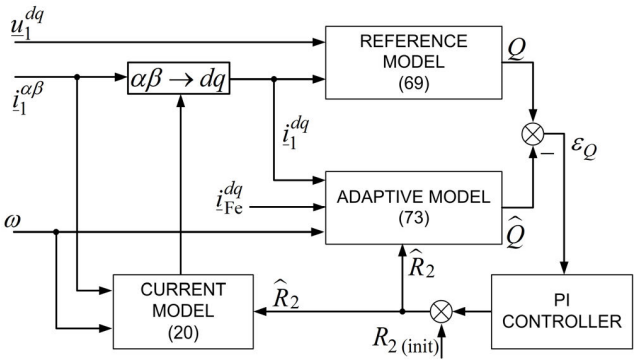

FIGURE 11. Modified reactive power MRAS for rotor resistance estimation.

TABLE 1. Induction machine nameplate data and nominal model parameters.

Nameplate Data		Model Parameters	
Nominal power	3.6 kW	Stator resistance	1.688 Ω
Nominal voltage	380 V	Rotor Resistance	3.685 Ω
Nominal current	11.5 A	Stator leakage inductance	0.0139 H
Nominal speed	935 min^{-1}	Rotor leakage inductance	0.0139 H
Number of poles	6	Magnetizing inductance	0.175 H
Winding connection	Y	Iron core resistance	520 Ω

In the iron loss compensation case, the estimated inductance converges to the actual value and is almost unaffected by the speed and torque change. However, if the iron losses are not compensated, the estimated inductance differs from the actual value. The difference is the lowest during the no-load conditions and further increases with the load. This confirms the results of earlier works where it was found that the error in rotor flux can have an increasing tendency with respect to the load then reach a maximum value to start further descending with increasing load [10].

Another simulation sequence was designed to test the ability of the estimator to track the change of the magnetizing inductance with the load:

- The magnetizing inductance in the FOC model is set to 110 % of the nominal value to simulate the parameter detuning. All other parameters are exact.
- The reference flux is set to the nominal value.
- The machine is started at 0.1 s to the nominal speed.
- Magnetizing inductance compensation is turned on at 1 s.
- At 2 s, the load torque starts to increase from zero to half of the nominal value linearly.
- The magnetizing inductance inside the IM model is modeled to decrease with the torque (also linearly).

The integral gain of the estimator is increased five times for better tracking performance which causes an overshoot at the beginning of the estimation process. The results are depicted in Fig. 14 and Fig. 16. In Fig. 15, the iron losses are compensated, and in Fig. 16, the compensation is inactive. In the case of the compensated iron losses, the estimator can track the change of the magnetizing inductance with the load almost perfectly. However, if the iron losses are not compensated, the estimator is able to monitor the monotonically decreasing trend, but the estimated value differs from the actual one. The difference is then increasing as the function of the increased torque.

The third simulation sequence tested the performance of the parallel operation of Q-MRAS and Lm-MRAS.

- The FOC model's magnetizing inductance and rotor resistance are set to 110 % and 120 %, respectively, of their nominal values to simulate the parameter detuning. All other parameters are exact.
- The reference flux is set to the nominal value.
- The machine is started at 0.1 s to the nominal speed.
- Half of the nominal load torque is applied at 1 s.
- Magnetizing inductance compensation is turned on at 2 s.
- Rotor resistance compensation is turned on at 4 s.

The Q-MRAS PI controller proportional and integral gains are set to 0.0001 and 0.03, respectively. The resulting magnetizing inductance and rotor resistance estimates are presented in Fig. 17 and Fig. 18. In Fig. 17, the iron losses are compensated, and in Fig. 18, the compensation is inactive. The results show that the rotor resistance detuning significantly influences the Lm-MRAS under load conditions. However, parallel operation with the Q-MRAS ensures that both the magnetizing inductance and rotor resistance are compensated correctly if the improved version with the iron losses is used. Again, the estimates are incorrect if the iron loss compensation is inactive, although both estimators successfully converge.

The last simulation sequence tested Lm-MRAS performance in a regenerative mode and during speed reversal.

- The magnetizing inductance in the FOC model is set to 110 % of the nominal value. All other parameters are exact.
- The reference flux is set to the nominal value.

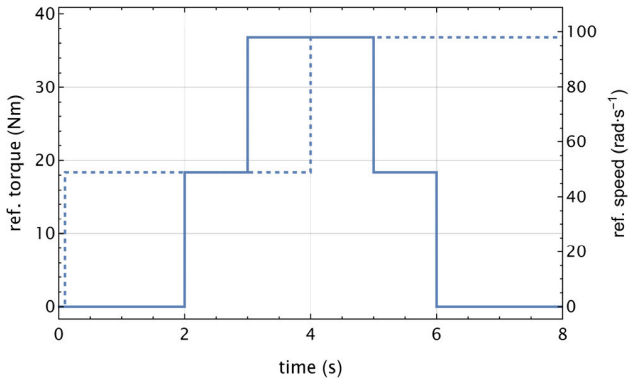

FIGURE 12. The simulated sequence of reference torque (solid) and speed (dashed).

- The machine is started at 0.1 s to the nominal speed. The sign of the reference speed is inverted, i.e., the drive is reversed at 4 s.
- Magnetizing inductance compensation is turned on at 1 s.
- Initially, the machine is unloaded. The load is increased to half of the nominal torque in a regenerative mode at 2 s. The machine is then unloaded at 3 s. At 5 s, the load increases to half of the nominal torque in a regenerative mode and decreases to zero at 5 s. Then, the machine is unloaded, and the load torque is increased to half of the nominal torque in a motoring mode at 7 s.

The time sequence of the step changes of the reference speed and torque is depicted in Fig. 19. The resulting magnetizing inductance estimates are depicted in Fig. 20 and Fig. 21. In Fig. 20, the iron losses are compensated, and in Fig. 21, the compensation is inactive. Overall, the simulation sequence confirms the ability of Lm-MRAS to estimate the magnetizing inductance in a four-quadrant operation of the drive. When the iron losses are compensated, slight variations in the estimated inductance value appear during the speed reversal. The variations during the change of the load are negligible. However, if the iron losses are not accounted for, the variation of the inductance increases, and the estimator operates with an error that depends on the loading of the machine.

VIII. EXPERIMENTAL RESULTS

The proposed Lm-MRAS estimator was also tested experimentally. The whole control algorithm was programmed in C language into Texas Instruments TMS320F28335 digital signal processor with the CPU clock set to 150 MHz. The calculation loop of the FOC is tied to the PWM frequency, which is selected to be 8 kHz. The data were sampled with a 400 μs period. The IM drive was loaded by an 8 kW DC motor supplied from a Siemens SINAMICS DCM converter. The experimental machine setup is depicted in Fig. 22.

For the motor current and DC-link voltage measurements, LEM LF 205-S with four conductor turns and LEM LV25-P,

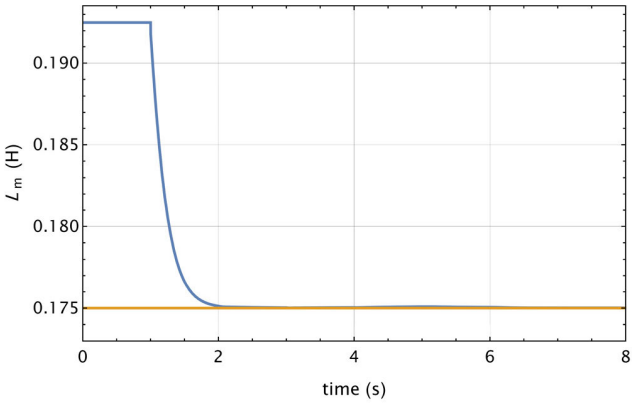

FIGURE 13. Estimated (blue) and actual (orange) magnetizing inductance during the step changes of speed and load; iron losses compensated.

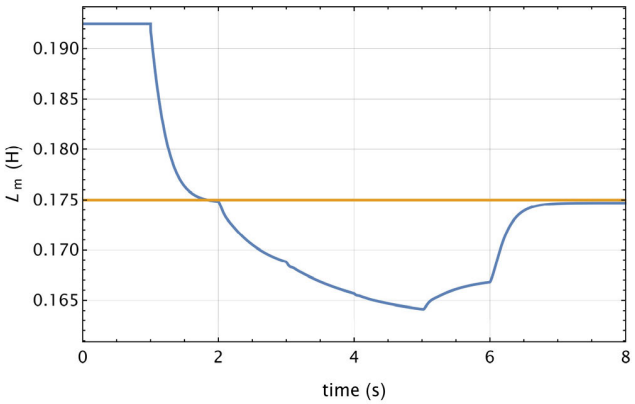

FIGURE 14. Estimated (blue) and actual (orange) magnetizing inductance during the step changes of speed and load; iron losses not compensated.

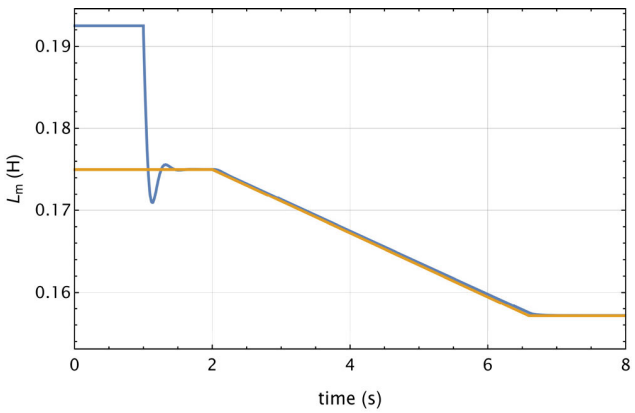

FIGURE 15. Estimated (blue) and actual (orange) magnetizing inductance. The magnetizing inductance in the motor model decreases as a function of torque; iron losses compensated.

respectively, were used along with our custom signal adjustment board. The board performs LEM output scaling via op-amp circuitry. All ADC conversions are synchronized with PWM and regularly triggered with a modulation period of 125 μs. As the machine supply converter, a standard three-phase two-level voltage-source inverter was utilized. The inverter is supplied from a diode rectifier that is connected

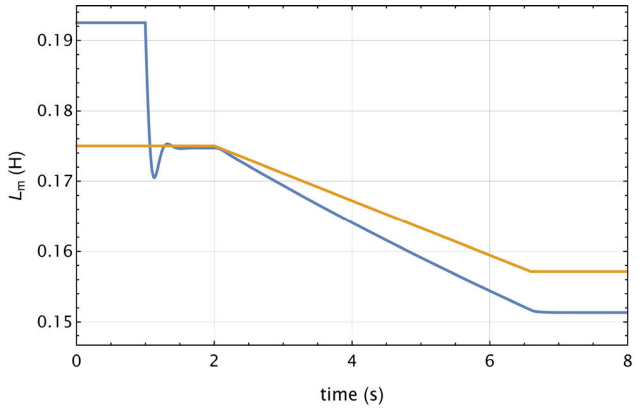

FIGURE 16. Estimated (blue) and actual (orange) magnetizing inductance. The magnetizing inductance in the motor model decreases as a function of torque; iron losses not compensated.

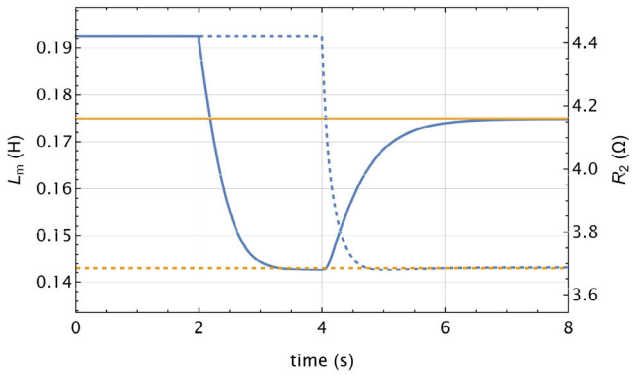

FIGURE 17. Parallel operation of Q-MRAS and Lm-MRAS. Estimated values (blue) and actual values (orange) of the magnetizing inductance (solid) and rotor resistance (dashed). Iron losses compensated. The load is applied at 1 s, Lm-MRAS is started at 2 s, and Q-MRAS is started at 4 s.

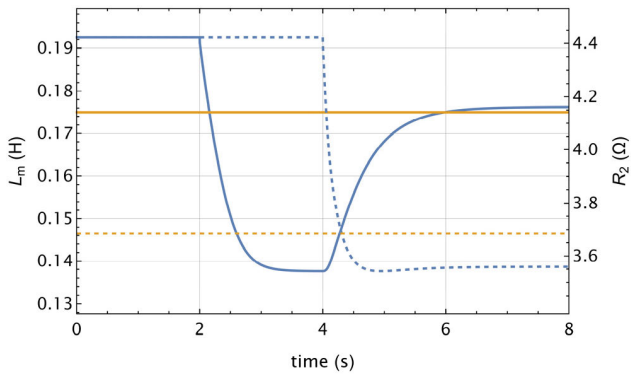

FIGURE 18. Parallel operation of Q-MRAS and Lm-MRAS. Estimated values (blue) and actual values (orange) of the magnetizing inductance (solid) and rotor resistance (dashed). Iron losses are not compensated. The load is applied at 1 s, Lm-MRAS is started at 2 s, and Q-MRAS is started at 4 s.

to a 400 V, 50 Hz AC grid. The rotor speed was measured using a LARM incremental encoder with 2500 pulses per revolution. The encoder output is scaled using the same signal

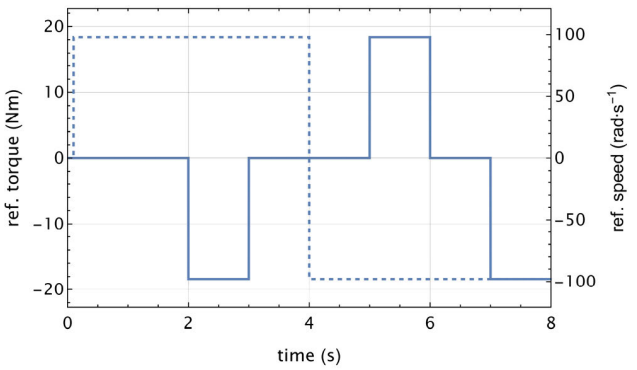

FIGURE 19. The simulated sequence of reference torque (solid) and speed (dashed) for a regenerative mode and speed reversal.

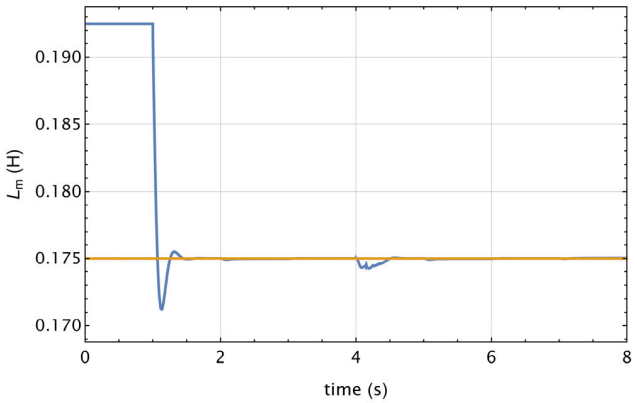

FIGURE 20. Estimated (blue) and actual (orange) magnetizing inductance for a regenerative mode and speed reversal; iron losses compensated.

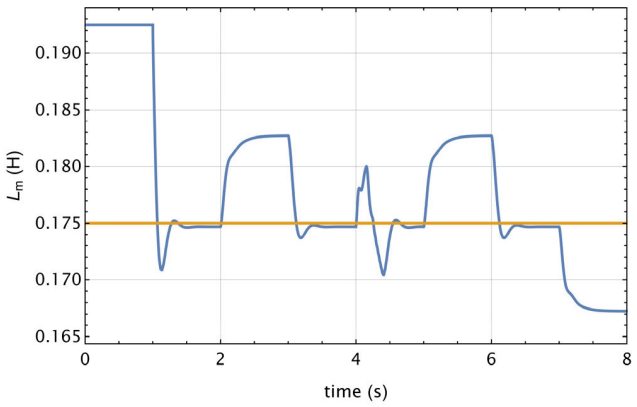

FIGURE 21. Estimated (blue) and actual (orange) magnetizing inductance for a regenerative mode and speed reversal; iron losses not compensated.

adjustment board and processed by the eQEP module of the TMS320F28335 DSP.

First, the no-load magnetizing characteristics in the form of the dependence of the magnetizing flux on the magnetizing current (i.e., $\psi_m = f\ (i_m)$) was measured during a no-load test from a 50 Hz supply with variable voltage amplitude. Because the utilized IM is a slip-ring type, the rotor winding was left open to rule out the influence of the rotor branch entirely.

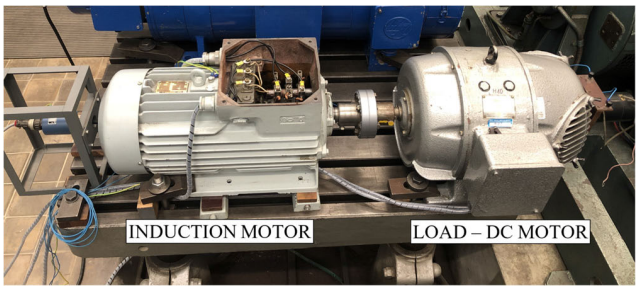

FIGURE 22. The tested induction motor and loading DC motor.

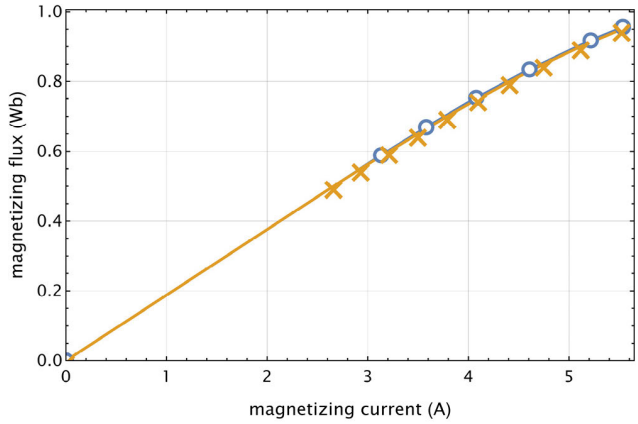

FIGURE 23. No-load magnetizing characteristics in the form $\psi_m = f\,(i_m)$ obtained from the modified no-load test (blue) and Lm-MRAS (orange).

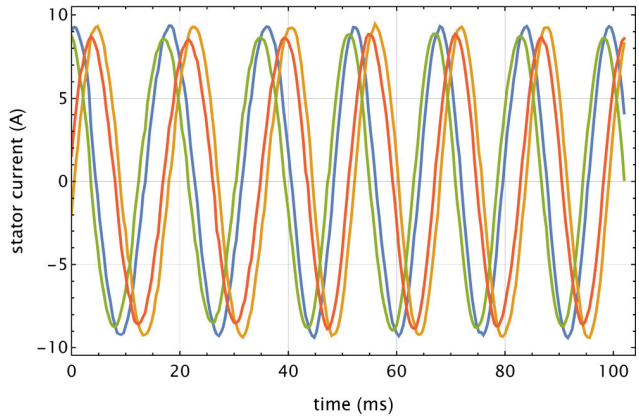

FIGURE 24. Measured α (blue) and β (orange) components of the stator current and estimated α (green) and β (red) components of the stator current. Nominal speed and rotor flux, half of the nominal load torque, iron loss compensation only.

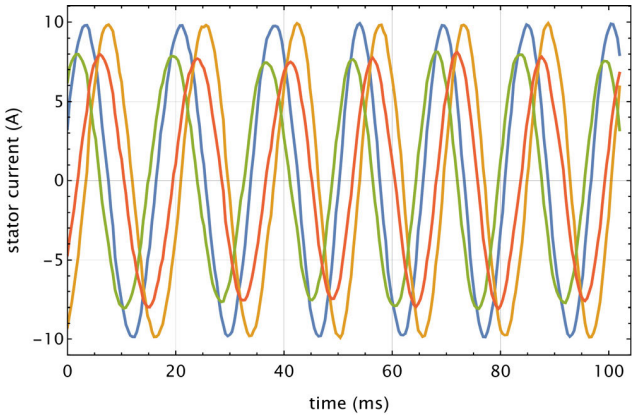

FIGURE 25. Measured α (blue) and β (orange) components of the stator current and estimated α (green) and β (red) components of the stator current. Nominal speed and rotor flux, half of the nominal load torque, iron loss and rotor resistance compensation.

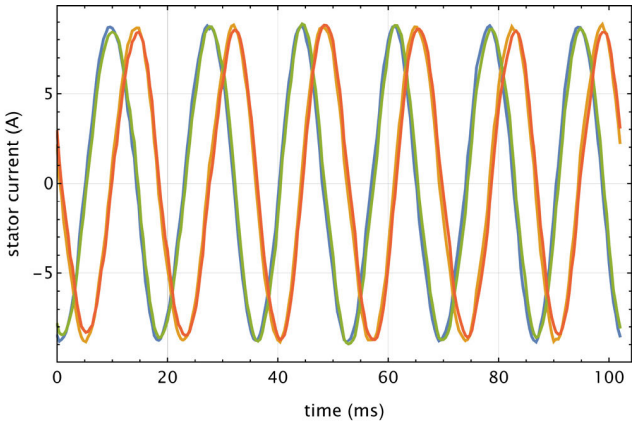

FIGURE 26. Measured α (blue) and β (orange) components of the stator current and estimated α (green) and β (red) components of the stator current. Nominal speed and rotor flux, half of the nominal load torque, iron loss, rotor resistance, and magnetizing inductance compensation.

To compare the no-load test results with the proposed Lm-MRAS, the unloaded drive was then connected to the inverter. To ensure a similar fundamental voltage frequency as during the no-load test, the reference speed was set to 104 rad·s^{-1}. Under the no-load conditions, the rotor current is close to zero, i.e., $i_2 \approx 0$ which, according to (8), means that the magnetizing flux is almost identical with the rotor flux, i.e., $\psi_\mathrm{m} \approx \psi_2$. Under these assumptions it is easy to obtain the magnetizing characteristics in the form $\psi_\mathrm{m} = f\,(i_\mathrm{m})$. The resulting comparison is depicted in Fig. 23. Out of the figure, it is evident that both the magnetizing characteristics are in excellent agreement.

To validate the performance of the parallel estimation of the magnetizing inductance and rotor resistance, the reference flux and speed were set to their nominal values and the load torque to half of the nominal value. Then, the actual and estimated $\alpha\beta$ current components were measured and calculated, respectively. The estimated currents were obtained using the current equation of the state-space model (33) transformed into $\alpha\beta$. The rotor flux vector components for the current estimator were obtained using (10).

The data were recorded for multiple cases. In all of them, the iron loss compensation was active. Also, between the measurements, the machine was stopped to cool back to ambient temperature. Fig. 24 shows the case when the Lm-MRAS was turned on at the beginning during the no-load operation to obtain the no-load value of the magnetizing inductance. Then the Lm-MRAS was deactivated,

and the drive was loaded with half of the nominal torque. Fig. 25 shows a similar case with the difference that only the rotor resistance compensation was active. Finally, Fig. 26 shows the case when both the magnetizing inductance and rotor resistance estimation were active.

Interestingly, the worst case is obtained when only the rotor resistance compensation is active. The incorrect value of the magnetizing inductance influences the Q-MRAS performance, leading to incorrectly estimated rotor resistance. If neither the magnetizing inductance nor the rotor resistance compensation is active, the results are better. However, it is expected that the resulting estimates would be worse after a long-time loading when the rotor temperature would be increased. The best match between the current components is obtained if all the compensations are active, indicating the correct estimation of the parameters.

IX. CONCLUSION

This paper presented a novel MRAS-type estimator with the included effect of iron losses and load. Despite the drawback that the reference model is not entirely free of the magnetizing inductance, the simulation and experimental results proved its ability to estimate the conventional and load-dependent magnetizing inductance saturation correctly. Furthermore, the estimator operation during load conditions was improved by introducing a simultaneously working reactive power MRAS with the included iron losses for the rotor resistance adaptation. It was found out that the influence of the iron losses on the accuracy of both parameters estimation becomes significant at higher loads.

Still, a few issues connected with the proposed estimation schemes should be acknowledged. First, it is assumed that the stator resistance and stator and rotor leakage inductance are known accurately. The stator resistance can be easily measured and corrected during the drive operation, but the leakage inductances cannot be measured directly. Furthermore, the rotor leakage inductance can also saturate as the function of the rotor current. One possibility of overcoming these problems would be adding a leakage inductance estimation through signal injection or recursive least-square methods.

Secondly, the iron losses were measured during the no-load operation. However, the iron losses are also dependent on the slip due to the different mutual speeds of the rotating magnetic field (fundamental component) and rotor. Furthermore, additional losses are present in the machine during load conditions. Therefore, the models and the estimates could be improved using a more sophisticated induction motor equivalent circuit.

Lastly, as mentioned in the beginning, the reference model is not free of magnetizing inductance. At this time, the authors are working on an improved estimator that eliminates this problem.

REFERENCES

[1] A. M. Bazzi and P. T. Krein, "Review of methods for real-time loss minimization in induction machines," *IEEE Trans. Ind. Appl.*, vol. 46, no. 6, pp. 2319–2328, Nov./Dec. 2010.

[2] Z. Peng, "Analysis and implementation of constrained MTPA criterion for induction machine drives," *IEEE Access*, vol. 8, pp. 176445–176453, 2020.

[3] Z. Qu, M. Ranta, M. Hinkkanen, and J. Luomi, "Loss-minimizing flux level control of induction motor drives," *IEEE Trans. Ind. Appl.*, vol. 48, no. 3, pp. 952–961, May/Jun. 2012.

[4] T. Tuovinen, M. Hinkkanen, and J. Luomi, "Modeling of saturation due to main and leakage flux interaction in induction machines," *IEEE Trans. Ind. Appl.*, vol. 46, no. 3, pp. 937–945, Jun. 2010.

[5] M. Hinkkanen, A.-K. Repo, M. Ranta, and J. Luomi, "Small-signal modeling of mutual saturation in induction machines," *IEEE Trans. Ind. Appl.*, vol. 46, no. 3, pp. 965–973, Jun. 2010.

[6] E. Molsa, S. E. Saarakkala, and M. Hinkkanen, "Influence of magnetic saturation on modeling of an induction motor," in *Proc. 13th Int. Conf. Electr. Mach. (ICEM)*, Sep. 2018, pp. 1572–1578.

[7] M. Ranta, M. Hinkkanen, E. Dlala, A.-K. Repo, and J. Luomi, "Inclusion of hysteresis and eddy current losses in dynamic induction machine models," in *Proc. IEEE Int. Electric Mach. Drives Conf.*, May 2009, pp. 1387–1392.

[8] K. Wang, R. Huai, Z. Yu, X. Zhang, F. Li, and L. Zhang, "Comparison study of induction motor models considering iron loss for electric drives," *Energies*, vol. 12, no. 3, p. 503, Feb. 2019.

[9] C. Mastorocostas, I. Kioskeridis, and N. Margaris, "Thermal and slip effects on rotor time constant in vector controlled induction motor drives," *IEEE Trans. Power Electron.*, vol. 21, no. 2, pp. 495–504, Mar. 2006.

[10] M. Sokola, "Vector control of induction machines using improved machine models," Ph.D. dissertation, School Eng., Liverpool John Moores Univ., Liverpool, U.K., 1998.

[11] J. Nerg, J. Pyrhonen, and J. Partanen, "Finite element modeling of the magnetizing inductance of an induction motor as a function of torque," *IEEE Trans. Magn.*, vol. 40, no. 4, pp. 2047–2049, Jul. 2004.

[12] D. C. Huynh, M. W. Dunnigan, and S. J. Finney, "On-line parameter estimation of an induction machine using a recursive least-squares algorithm with multiple time-varying forgetting factors," in *Proc. IEEE Int. Conf. Power Energy*, Nov. 2010, pp. 444–449.

[13] R. P. R. Siddavatam and U. Loganathan, "Identification of induction machine parameters including core loss resistance using recursive least mean square algorithm," in *Proc. 45th Annu. Conf. IEEE Ind. Electron. Soc. (IECON)*, Oct. 2019, pp. 1095–1100.

[14] H. Zhao, H. H. Eldeeb, J. Wang, J. Kang, Y. Zhan, G. Xu, and O. A. Mohammed, "Parameter identification based online noninvasive estimation of rotor temperature in induction motors," *IEEE Trans. Ind. Appl.*, vol. 57, no. 1, pp. 417–426, Jan. 2021.

[15] S. A. Bednarz and M. Dybkowski, "Estimation of the induction motor stator and rotor resistance using active and reactive power based model reference adaptive system estimator," *Appl. Sci.*, vol. 9, no. 23, p. 5145, Nov. 2019.

[16] P. Cao, X. Zhang, and S. Yang, "A unified-model-based analysis of MRAS for online rotor time constant estimation in an induction motor drive," *IEEE Trans. Ind. Electron.*, vol. 64, no. 6, pp. 4361–4371, Jun. 2017.

[17] M. Dybkowski, "Universal speed and flux estimator for induction motor," *Power Electron. Drives*, vol. 3, no. 1, pp. 157–169, Dec. 2018.

[18] S. Maiti, C. Chakraborty, Y. Hori, and M. C. Ta, "Model reference adaptive controller-based rotor resistance and speed estimation techniques for vector controlled induction motor drive utilizing reactive power," *IEEE Trans. Ind. Electron.*, vol. 55, no. 2, pp. 594–601, Feb. 2008.

[19] P. Cao, X. Zhang, S. Yang, Z. Xie, and Y. Zhang, "Reactive-power-based MRAS for online rotor time constant estimation in induction motor drives," *IEEE Trans. Power Electron.*, vol. 33, no. 12, pp. 10835–10845, Dec. 2018.

[20] L. Liu, Y. Guo, and J. Wang, "Online identification of mutual inductance of induction motor without magnetizing curve," in *Proc. Annu. Amer. Control Conf. (ACC)*, Jun. 2018, pp. 3293–3297.

[21] F. L. Mapelli, D. Tarsitano, and F. Cheli, "A rotor resistance MRAS estimator for EV induction motor traction drive based on torque and reactive stator power: Simulation and experimental results," in *Proc. Int. Conf. El. Mach. (ICEM)*, Berlin, Germany, 2014, pp. 31–37.

[22] K. R. Cho and J. K. Seok, "Induction motor rotor temperature estimation based on a high-frequency model of a rotor bar," *IEEE Trans. Ind. Appl.*, vol. 45, no. 4, pp. 1267–1275, Jul. 2009.

[23] F. Baneira, A. G. Yepes, O. López, and J. Doval-Gandoy, "Estimation method of stator winding temperature for dual three-phase machines based on DC-signal injection," *IEEE Trans. Power Electron.*, vol. 31, no. 7, pp. 5141–5148, Jul. 2016.

[24] F. Briz, M. W. Degner, J. M. Guerrero, and A. B. Diez, "Temperature estimation in inverter fed machines using high frequency carrier signal injection," in *Proc. IEEE Ind. Appl. Annu. Meeting*, Sep. 2007, pp. 2030–2037.
[25] S. M. N. Hasan and I. Husain, "A Luenberger–sliding mode observer for online parameter estimation and adaptation in high-performance induction motor drives," *IEEE Trans. Ind. Appl.*, vol. 45, no. 2, pp. 772–781, Apr. 2009.
[26] S. Yang, D. Ding, X. Li, Z. Xie, X. Zhang, and L. Chang, "A novel online parameter estimation method for indirect field oriented induction motor drives," *IEEE Trans. Energy Convers.*, vol. 32, no. 4, pp. 1562–1573, Dec. 2017.
[27] E. Zerdali, "A comparative study on adaptive EKF observers for state and parameter estimation of induction motor," *IEEE Trans. Energy Convers.*, vol. 35, no. 3, pp. 1443–1452, Sep. 2020.
[28] O. Çetin, A. Dalcalı, and F. Temurtaş, "A comparative study on parameters estimation of squirrel cage induction motors using neural networks with unmemorized training," *Eng. Sci. Technol., Int. J.*, vol. 23, no. 5, pp. 1126–1133, Oct. 2020.
[29] M. Wlas, Z. Krzeminski, and H. A. Toliyat, "Neural-network-based parameter estimations of induction motors," *IEEE Trans. Ind. Electron.*, vol. 55, no. 4, pp. 1783–1794, Apr. 2008.
[30] T. P. Van, D. V. Tien, Z. Leonowicz, M. Jasinski, T. Sikorski, and P. Chakrabarti, "Online rotor and stator resistance estimation based on artificial neural network applied in sensorless induction motor drive," *Energies*, vol. 13, no. 18, p. 4946, Sep. 2020.
[31] M. Sokola and E. Levi, "A novel induction machine model and its application in the development of an advanced vector control scheme," *Int. J. Elect. Eng. Educ.*, vol. 37, no. 3, pp. 48–233, Jul. 2000.
[32] M. Korzonek, G. Tarchala, and T. Orlowska-Kowalska, "A review on MRAS-type speed estimators for reliable and efficient induction motor drives," *ISA Trans.*, vol. 93, pp. 1–13, Oct. 2019.
[33] A. Pal, S. Das, and A. K. Chattopadhyay, "An improved rotor flux space vector based MRAS for field-oriented control of induction motor drives," *IEEE Trans. Power Electron.*, vol. 33, no. 6, pp. 5131–5141, Jun. 2018.
[34] H. Karkkainen, L. Aarniovuori, M. Niemela, and J. Pyrhonen, "Converter-fed induction motor efficiency: Practical applicability of IEC methods," *IEEE Ind. Electron. Mag.*, vol. 11, no. 2, pp. 45–57, Jun. 2017.
[35] M. Koteich, "Flux estimation algorithms for electric drives: A comparative study," in *Proc. 3rd Int. Conf. Renew. Energies Developing Countries (REDEC)*, Jul. 2016, pp. 1–6.
[36] Y. Wang, W. Xie, X. Wang, and D. Gerling, "A precise voltage distortion compensation strategy for voltage source inverters," *IEEE Trans. Ind. Electron.*, vol. 65, no. 1, pp. 59–66, Jan. 2018.
[37] O. Lipcak and J. Bauer, "Analysis of voltage distortion and comparison of two simple voltage compensation methods for sensorless control of induction motor," in *Proc. IEEE 10th Int. Symp. Sensorless Control Electr. Drives (SLED)*, Sep. 2019, pp. 1–6.

ONDREJ LIPCAK (Graduate Student Member, IEEE) was born in Prague, Czech Republic, in 1993. He received the M.S. degree in electrical machines, apparatus and drives from Czech Technical University in Prague (CTU), in 2018, where he is currently pursuing the Ph.D. degree in electrical machines and drives with the Department of Electric Drives and Traction, Faculty of Electrical Engineering.

Since 2018, he has been involved in research and teaching activities with the Department of Electric Drives. His research interests include mathematical modeling, parameter estimation, and efficient control of AC machines.

JAN BAUER (Member, IEEE) was born in Prague, Czech Republic, in 1983. He received the M.S. and Ph.D. degrees in electrical engineering from Czech Technical University in Prague (CTU), in 2007 and 2015, respectively.

He is currently an Assistant Professor with the Department of Electric Drives and Traction, Faculty of Electrical Engineering, CTU. His research interests include the control of electric drives and power converters with the aim of efficiency increase.